Supplementary Information

The Electrochemical Failure Mechanisms Investigation of the $Li_{1+x}Al_xTi_{2-x}(PO_4)_3$

Solid-State Electrolytes

Can Huang, Fang Wang, Shuo Huang, Jianhe Hong, Shuoguo Yuan, Shuen Hou,

Hongyun Jin*

Engineering Research Center of Nano-Geo Materials of Ministry of Education,

Faculty of Materials Science and Chemistry, China University of Geosciences,

Wuhan 430074, China

Table S1. Cell parameters of LATP pellet obtained by Refinement of XRD results.

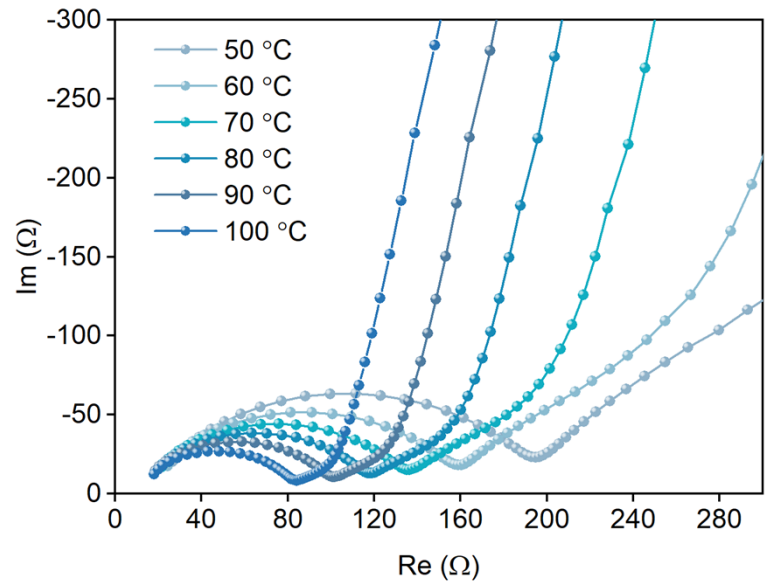| composition	a (Å)	c (Å)	α (°)	γ (°)
$Li_{1.4}Al_{0.4}Ti_{1.6}(PO_4)_3$	8.49763	20.79888	90	120

Fig. S1. Nyquist plot of LATP at different temperatures.

Table S2. Electrochemical impedance spectra fitting results of LATP pellet at different temperature.

temperature (°C)	impedance (Ω)	ionic conductivity (S cm^{-1})
50	188.3	3.9716×10^{-4}
60	152.3	4.9103×10^{-4}
70	129.9	5.7571×10^{-4}
80	112.3	6.6593×10^{-4}
90	95.29	7.8481×10^{-4}
100	77.46	9.6546×10^{-4}

Table S3. Electrochemical impedance spectra fitting results of the Li/LATP/LFP batteries.

cycle number	R_{bulk} (Ω)	R_{SEI} (Ω)	R_{ct} (Ω)
0	11.43	17.15	66.41
10	19.69	79.66	177.7
20	46.46	98.55	227.2
30	48.81	150.6	300.9
40	51.54	276.8	556.2
50	51.94	355.2	845.8

Table S4. Lithium diffusion coefficient of the Li/LATP/LFP batteries.

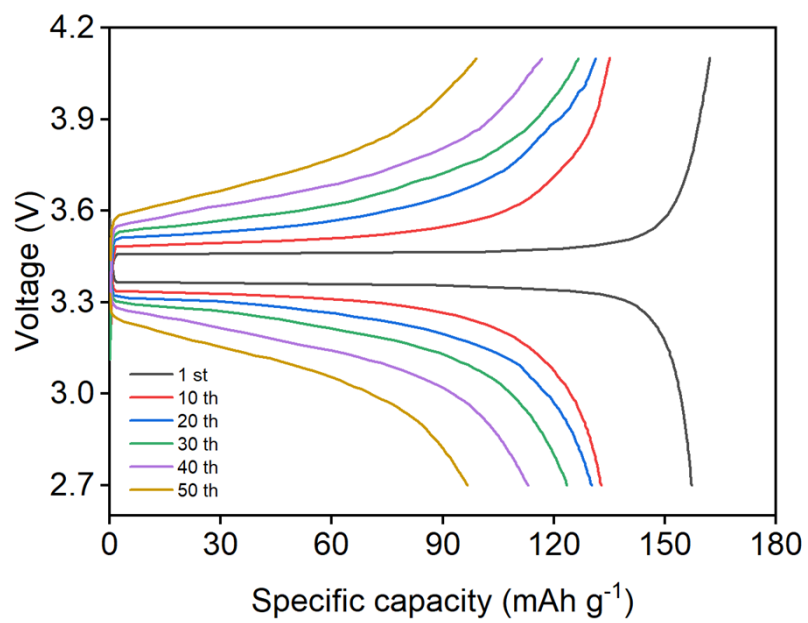| cycle number	A_w ($\Omega\ s^{-1/2}$)	D_{Li+} ($cm^2\ s^{-1}$)
0	33.67886	1.8743×10^{-13}
10	72.0356	4.0969×10^{-14}
20	92.39058	2.4905×10^{-14}
30	108.60832	1.8023×10^{-14}
40	182.81896	6.3607×10^{-15}
50	197.09131	5.4728×10^{-15}

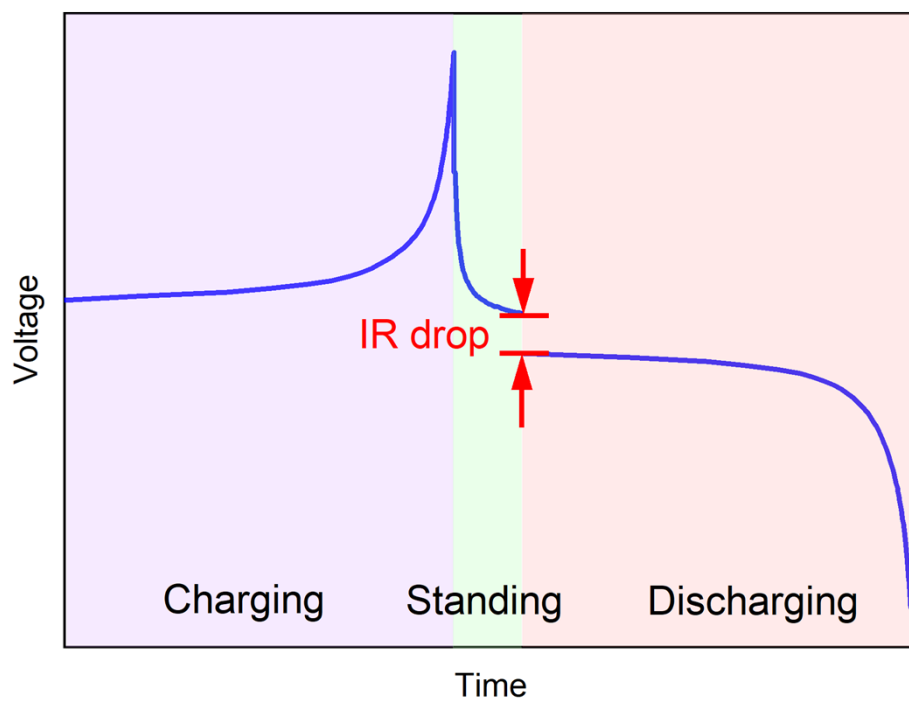**Fig. S2**. The charge-discharge profiles of the Li/LATP/LFP batteries.

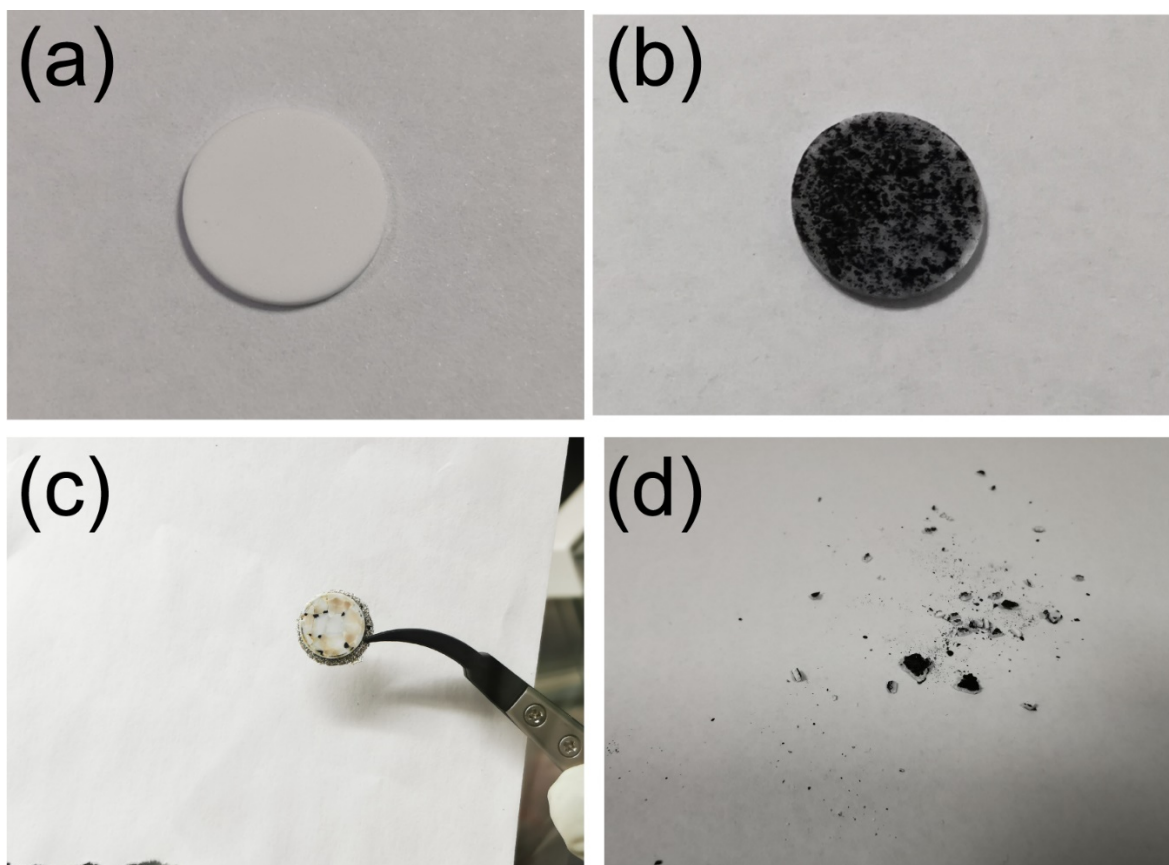**Fig. S3** illustration of IR drop.

Fig. S4. Digital photos of (a) LATP pellet before cycling, (b) anode side of the LATP pellet after 2 cycles, (c) cathode side of LATP pellet after 50 cycles. Obvious cracks can be found on the surface of the cathode side of the LATP pellet after 50 cycles. The pellet did not collapse because of the restriction of the Li metal anode and the foamed nickel. After removing the Li metal anode and the foamed nickel (caught in the tweezers), the LATP pellet collapsed into pieces, as shown in (d) that exhibited the anode side of LATP pellet after 50 cycles.

Fig. S5. Digital image of the decomposed LATP powder obtained from the surface of
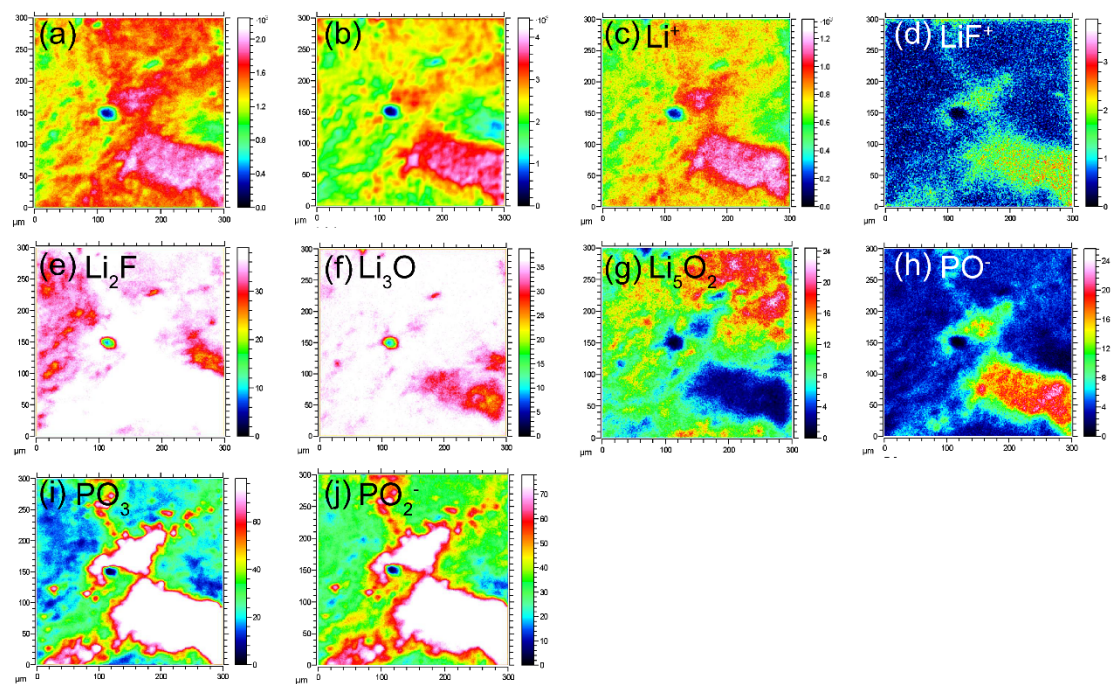
the reacted LATP pellets.

Fig. S6. TOF-SIMS results of the LATP pellet after 2 cycles. the total element distribution of (a) positive ion mode, and (b) negative ion mode. The distribution of (c) Li^+, (d) LiF^+, (e) Li_2F, (f) Li_3O, (g) Li_5O_2, (h) PO^-, (i) PO_3, and (j) PO_2^-.

Table S5. Maximum stress at different volume expansion ration obtained by FEA.

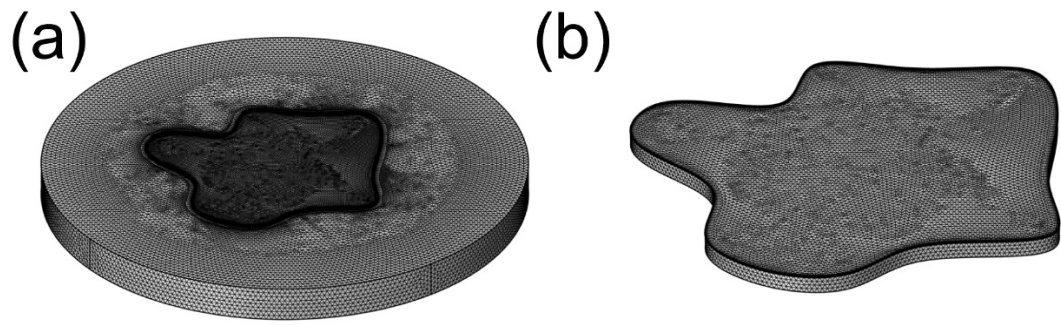| expansion ratio (%)	maximum stress in degradation region (GPa)	maximum stress at interface region (GPa)
4	8.821	11.57
6	13.23	17.35
8	17.64	23.13
10	22.05	28.91
12	26.46	34.70
14	30.87	40.48
16	35.28	46.26
18	39.70	52.05
20	44.11	57.83
22	48.52	63.61
24	52.93	69.39

Fig. S7. Meshing of (a) LATP pellet and (b) enlarged decomposition region in

COMSOL.

Table S6. The parameters for FEA in COMSOL.

	parameter	value	unit
	Radius	55	mm
	Thickness	8	mm
LATP pellet	Density	2.95	$g\ cm^{-3}$
	Poisson's ratio	0.25	
	Young's modulus	192	GPa
	Area (% of surface)	20	
	Thickness	2	mm
Degradation region	Density	2.95	$g\ cm^{-3}$
	Poisson's ratio	0.25	
	Young's modulus	112	GPa